JACS
JOURNAL OF THE AMERICAN CHEMICAL SOCIETY

pubs.acs.org/JACS

Article

A Porphyrinic Zirconium Metal–Organic Framework for Oxygen Reduction Reaction: Tailoring the Spacing between Active-Sites through Chain-Based Inorganic Building Units

Magdalena Ola Cichocka,[▽] Zuozhong Liang,[▽] Dawei Feng, Seoin Back, Samira Siahrostami, Xia Wang, Laura Samperisi, Yujia Sun, Hongyi Xu, Niklas Hedin, Haoquan Zheng,* Xiaodong Zou, Hong-Cai Zhou,* and Zhehao Huang*

Cite This: *J. Am. Chem. Soc.* 2020, 142, 15386–15395

Read Online

ACCESS | Metrics & More | Article Recommendations | Supporting Information

ABSTRACT: The oxygen reduction reaction (ORR) is central in carbon-neutral energy devices. While platinum group materials have shown high activities for ORR, their practical uses are hampered by concerns over deactivation, slow kinetics, exorbitant cost, and scarce nature reserve. The low cost yet high tunability of metal–organic frameworks (MOFs) provide a unique platform for tailoring their characteristic properties as new electrocatalysts. Herein, we report a new concept of design and present stable Zr-chain-based MOFs as efficient electrocatalysts for ORR. The strategy is based on using Zr-chains to promote high chemical and redox stability and, more importantly, tailor the immobilization and packing of redox active-sites at a density that is ideal to improve the reaction kinetics. The obtained new electrocatalyst, PCN-226, thereby shows high ORR activity. We further demonstrate PCN-226 as a promising electrode material for practical applications in rechargeable Zn-air batteries, with a high peak power density of 133 mW cm^{-2}. Being one of the very few electrocatalytic MOFs for ORR, this work provides a new concept by designing chain-based structures to enrich the diversity of efficient electrocatalysts and MOFs.

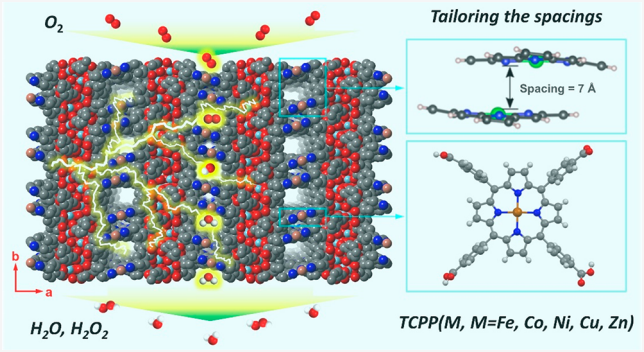

INTRODUCTION

The increasing global demands for sustainable energy simultaneously drive the development of new devices for energy conversion. The oxygen reduction reaction (ORR) plays a crucial role in such type of devices including fuel cells and metal-air batteries.[1,2] Platinum group materials are the predominant class of materials that are used as electrocatalysts for ORR.[3] However, their scarcity, high cost, low reaction kinetics, and stability prevent their widespread implementation in commercial green energy applications. Thus, driven by the crucial importance of the ORR in energy conversion processes, numerous systems based on nonprecious elements have been developed in the search for low-cost and stable candidates with good electrocatalytic activities.[4−8] In addition, high surface area scaffolds are paramount in the development of electrocatalysts for their implementations in various practical devices concerning deactivation, recyclability, and water solubility.

Metal–organic frameworks (MOFs) are porous inorganic–organic hybrid materials with extraordinarily high surface areas.[9,10] With high accessibility to the active-sites, MOFs take on dual roles and act as both catalysts and porous supports in heterogeneous catalysis. Notably, immobilizing catalytic sites in the well-defined structures can effectively limit deactivation pathways.[11,12] An important advantage of MOFs as compared to carbon and metal oxides-based materials is the possibility to easily and systematically design and alter the pores size and functionality at a molecular level by applying reticular chemistry.[13] As compared to noble metals, which are mostly nonporous, the fast mass transport inside crystals, as well as their low cost, endow MOFs as a promising class of materials in the energy storage and conversion field.[14−20] To further tackle their charge transport ability, MOFs have been designed either by orbital overlapping and charge delocalization between linkers[21−26] or by introducing redox-active molecular linkers.[27−29] Metalloporphyrin complexes exhibit strong interactions with O_2 and offer a good opportunity by serving as a channel for electron transfer via a hopping mechanism.[30−32]

Received: June 11, 2020
Published: August 10, 2020

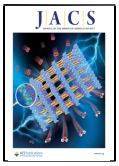

https://dx.doi.org/10.1021/jacs.0c06329
J. Am. Chem. Soc. 2020, 142, 15386–15395

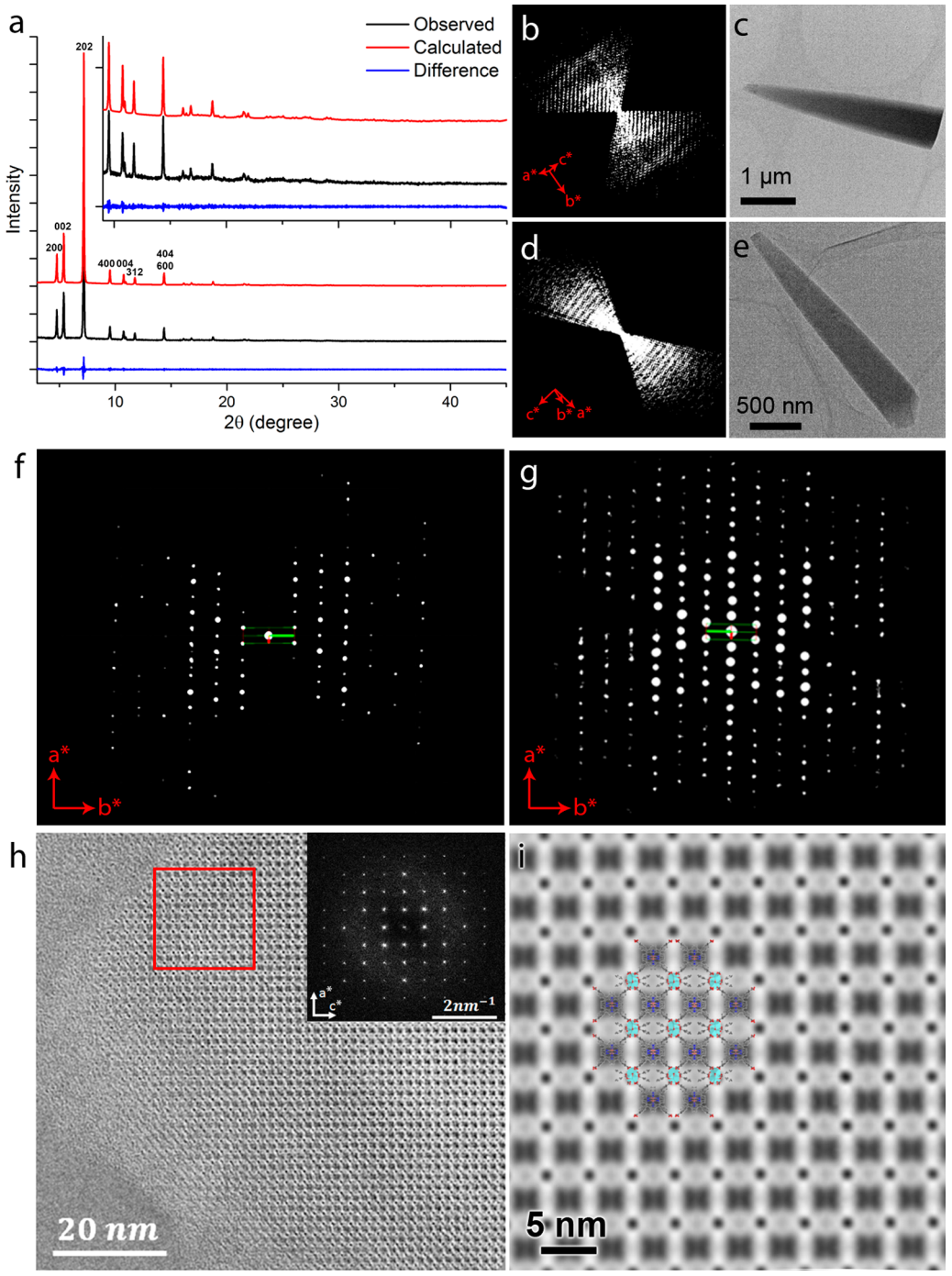

Figure 1. (a) Pawley fit of the experimental PXRD pattern (λ = 1.5406 Å) of PCN-226, which shows a good agreement. (b and d) Reconstructed 3D reciprocal lattice of PCN-226(Cu) and PCN-226(Co), respectively. (c and e) The particles from which the cRED data were collected. (f and g) The *hk*0 reciprocal planes of PCN-226(Cu) and PCN-226(Co), respectively, showing a similar intensity distribution. (h) HRTEM image of PCN-226(Cu) along the [010] direction that shows a rectangular pore packing with d_{200} = 18.32 Å and d_{002} = 16.18 Å (calculated d_{200} = 18.53 Å and d_{002} = 16.25 Å). Inset: Fourier transform of the image. (i) Symmetry imposed HRTEM image from the region highlighted by the red square in (h). The structural model of PCN-226(Cu) is superimposed in the image to show the good agreement.

Moreover, the rich chemistry and the high electrochemical stability of metalloporphyrin complexes endow porphyrinic MOFs as designable and durable electrocatalysts. Recently, such MOFs have been successfully utilized for the electrocatalytic hydrogen evolution reaction (HER),[33,34] CO_2 reduction reaction (CO_2RR),[35−37] oxygen evolution reaction (OER),[38−40] and oxygen reduction reaction (ORR),[41−44] etc. By efficiently limiting the deactivation pathways related to the electrocatalytic sites, these MOFs show electrochemical activities and relatively stable cycling. However, the structural and chemical stabilities of MOFs and, more importantly, the sparse active-sites in most studied MOFs are the major drawbacks, which have rendered such MOFs with limited redox capabilities.

Herein, we report the design of a new MOF, denoted PCN-226, which is built by linking redox-active metalloporphyrins

https://dx.doi.org/10.1021/jacs.0c06329
J. Am. Chem. Soc. 2020, 142, 15386−15395

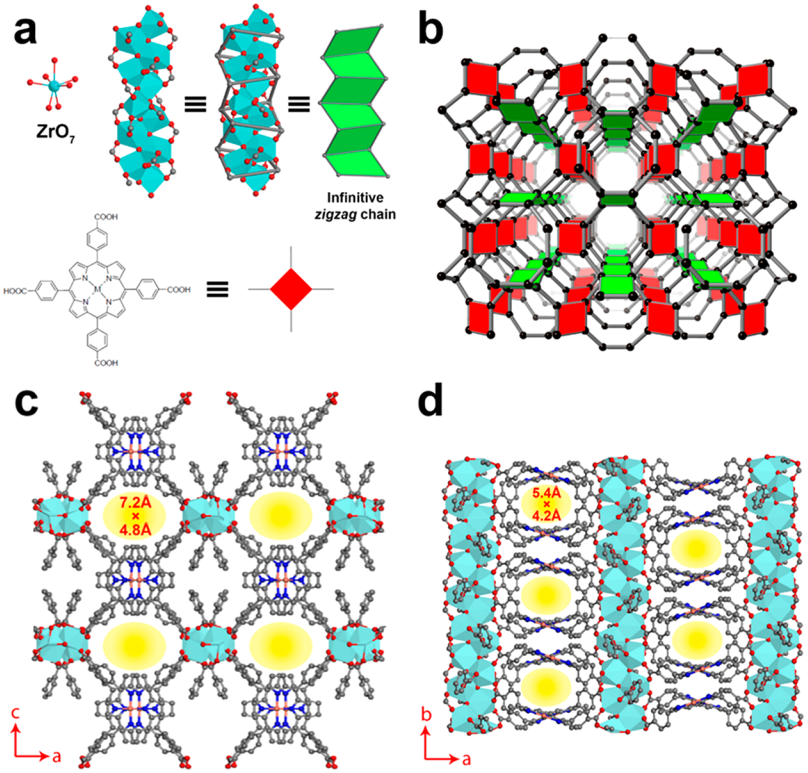

Figure 2. (a) PCN-226 is formed by the linkage of infinite zigzag zirconium chains and TCPP. The infinite zigzag zirconium chains have the composition $[ZrO(-COO)_2]_\infty$, with Zr atoms being hepta-coordinated. (b) The connection of PCN-226 showing a new topology, **ztt**, with Schlafli symbol $\{4\cdot8^2\}\{4^2\cdot6\cdot8^2\cdot10\}$ for the net. (c) The crystal structure of PCN-226 viewed along the *b*-axis showing the pore opening 7.2 Å × 4.8 Å and (d) the crystal structure viewed along the *c*-axis showing the 5.4 Å × 4.2 Å opening pores. Cyan capped octahedral, Zr; red spheres, O; black spheres, C, blue spheres, N; orange spheres, Cu.

and Zr(+4) cations. Use of earth abundant elements significantly reduces the producing cost as compared to use of noble metal-based materials. Moreover, according to the hard soft acid base (HSAB) theory, Zr(+4) cations have strong affinity with carboxyl-functionalized metalloporphyrins and are able to produce stable MOFs.[45] In addition to the stable, accessible, and redox active-sites for ORR, the MOF was designed uniquely on the basis of an infinite zigzag Zr-oxide chain structure. The chain-based structure not only enhances the overall stability of the MOF but also allows the redox active-sites at a close space to give rise to high reaction kinetics and catalyst loadings. The density of catalytically active-sites of PCN-226 is the highest among the reported porphyrinic Zr-MOFs. We prepared PCN-226 nanocrystals to improve the diffusion kinetics of adsorbed and reacting molecules. The structure of PCN-226 was determined by continuous rotation electron diffraction (cRED),[46,47] also known as microcrystal electron diffraction (MicroED).[48] As an electrocatalyst for ORR, PCN-226 showed high activity and reaction kinetics, especially as compared to cluster-based MOFs. When applied as electrodes for practical application in a rechargeable Zn-air battery, PCN-226 exhibited a high peak power density of 133 mW cm^{-2}. The integrity of PCN-226 remained intact after ORR.

RESULTS AND DISCUSSION

Synthesis and Characterization. The Zr-chain building units have first been reported in the MIL-140 series.[49] Because of the high connectivity of Zr and the robustness of the oxide chain unit, these structures show high mechanical, thermal, and hydrothermal stability as compared to the UiO series Zr-MOFs based on the Zr_6-oxo cluster.[49] Yet, such Zr-oxide chain structure has been found so far only in MIL-140 and MIL-163 and their derivatives,[49,50] presumably due to the lack of rationale for the synthesis of such a building unit. In particular, in the reported porphyrinic Zr-MOFs, the Zr_6-oxo cluster ($ZrO_4(OH)_4$) is dominating and adopts versatile connecting modes and yields different structures with outstanding stabilities.[51−58] Because of the large size of the porphyrnic linker, the metalloporphyrin centers in these structures are isolated by the Zr_6-oxo nodes, which prevents collaborative catalytic processes in the frameworks. To avoid the formation of the Zr_6-oxo phases, we herein adopt a thermodynamically controlled synthesis to enforce the formation of the Zr-oxide chain structure. Specifically, we conducted the reaction at a higher temperature (140 °C) than that in a typical Zr-MOF synthesis and added a high excess of benzoic acid (BA, BA/Zr = 67, molar ratio) as a competing reagent. As the BA can competitively coordinate to Zr atoms to control both the kinetics and the thermodynamics of the Zr-MOF formation (Scheme S2), a large amount of BA can inhibit the formation of Zr_6-oxo containing structures with lower thermodynamic stability. Meanwhile, higher reaction temperatures can facilitate the formation of Zr chains by overcoming the associated higher energetic barrier, as compared to the formation of kinetically favored Zr_6 clusters in typical Zr-MOFs. As expected, we obtained a Zr-oxide chain-based framework PCN-226. By applying the same strategy, isostructural MOFs with uncoordinated porphyrin and different metalloporphyrins, containing ions of metals such as Cu, Co, Ni, Fe, and Zn,

https://dx.doi.org/10.1021/jacs.0c06329
J. Am. Chem. Soc. 2020, 142, 15386−15395

have been successfully obtained, to create a new series of ultrastable porphyrinic Zr-MOFs.

The resulting MOF, PCN-226(Cu), was characterized by powder X-ray diffraction (PXRD), which shows the high crystallinity of the MOF with intense and sharp peaks (Figure 1a). Moreover, the features in the PXRD patterns (Figure S1) show that a series of isostructural PCN-226s could be synthesized with the same structure and topology. Scanning electron microscopy (SEM) images show a plank-like crystal morphology of the MOF with a 1−20 μm length and ca. 500 nm thickness (Figure S2). Continuous rotation electron diffraction (cRED) was applied for ab initio structure determination of PCN-226(Cu) and PCN-226(Co), respectively. The unit cell parameters obtained from the cRED data were refined against PXRD data by using the Pawley method, and the structural models were refined against the cRED data (Figures 1b−g, S3, and S4 and Tables S1−3; see the Supporting Information for more details). The refinement results further confirm that the PCN-226's have the same structure. As expected from our synthetic strategy, the three-dimensional (3D) structure is constructed by linking infinite zigzag ZrO_7 chains with metalloporphyrin molecules (Figure 2). Interestingly, besides the carboxylates from metalloporphyrin, BAs were also connected to the Zr-oxo chains (Figure S5). This connection indicates the importance of using excessive BAs in the synthesis, where BAs inhibit the formation of Zr_6-oxo clusters and favor the formation of Zr-oxide chains by coordinating to the Zr(+4) cations. To the best of our knowledge, the unique chain structure endows PCN-226 with a novel topology **ztt** that has never been reported. The metal loadings in the porphyrins of PCN-226(Cu) and PCN-226(Co) were 79.4% and 87.2%, respectively, which was calculated from inductively coupled plasma optical emission spectroscopy (ICP-OES) (Table S4).

PCN-226 contains two topologically distinct yet interconnected channels along the [010] and [001] directions, respectively (Figures 2c,d and S6). The chain-based structure effectively limits the spacing and results in a high packing density of metalloporphyrins, where the electrochemical active-sites are loaded. On the basis of the crystal structures, the packing density of PCN-226 is 1.4−11.0 times higher as compared to those of other reported porphyrinic Zr-MOFs (Table 1). HRTEM images clearly show the rectangular pore arrangement (Figure 1h and i), which is in good agreement with the structural model. The permanent porosity of PCN-226 was further estimated by analysis of the N_2 sorption isotherm at 77 K. A N_2 uptake of 10.1 mmol g^{-1} and a Brunauer−Emmett−Teller (BET) surface area of 800 m^2 g^{-1} were calculated for PCN-226(Cu) (Figure S7). The experimental surface area was slightly larger than the theoretical value of PCN-226(Cu) of 621 m^2 g^{-1} based on the structural model, which indicated the formation of possible defects with missing linkers. Simulation from the N_2 adsorption isotherm based on nonlocal density functional theory (NLDFT) gave a pore size distribution in the range of 5.3−7.8 Å. Other PCN-226 MOFs with different metalloporphyrins show similar N_2 uptake, surface area, and pore size distribution (Figures S8−S12).

As compared to the isolated clusters, the highly connected chain structures provide enhanced stability by resisting the attack of water and other guest species.[49] We tested the chemical stabilities of PCN-226 using reported procedures in the MOF field.[18,49] It exhibited remarkable stabilities of PCN-226 in aqueous solutions in a wide pH range (1−13) for at least 7 days (Figures S13 and S14), as a result of the combination of chain structure and strong Zr(+4)−O bonding. PCN-226 showed very little leaching (<0.97%) in acidic and basic conditions, as calculated from the UV−vis spectra of PCN-226 measured at different pH values (pH 1−3 and 11−13) for 7 days (Figures S15−S18). Thermogravimetric analysis (TGA) showed PCN-226(Cu) was stable up to at least 400 °C (Figure S19). After the first weight loss before 100 °C due to the removal of guest molecules, only ∼2% of the total framework weight was lost before the ligands started combustion at above 400 °C. This shows the chain-containing PCN-226 is much more stable than the cluster-containing Zr-MOFs, which undergo dehydroxylation at a much lower temperature (∼250 °C).[29,45]

Table 1. Comparison of the Density of Catalytically Active-Sites of PCN-226 with the Most Reported Porphyrinic Zr-MOFs

Zr-metallo-porphyrin MOF	building unit	topology	density (10^8 porphyrinic metal sites μm^{-3})[b]	ref
PCN-226	ZrO_7 zigzag chain	new[a]	5.91	this work
PCN-221	$Zr_8(\mu_4\text{-O})_6$ cluster	**ftw**	4.04	51
MOF-525	$Zr_6(\mu_3\text{-O})_4(\mu_3\text{-OH})_4$ cluster	**ftw**	4.11	52
PCN-222	$Zr_6(\mu_3\text{-OH})_8$ cluster	**csq**	2.29	53
MOF-545	$Zr_6(\mu_3\text{-O})_8$ cluster	**csq**	2.28	52
PCN-223	$Zr_6(\mu_3\text{-O})_4(\mu_3\text{-OH})_4$ cluster	**shp**	4.47	54
PCN-224	$Zr_6(\mu_3\text{-O})_4(\mu_3\text{-OH})_4$ cluster	**she**	2.10	55
PCN-225	$Zr_6(\mu_3\text{-O})_4(\mu_3\text{-OH})_4$ cluster	**sqc**	3.72	56
PCN-228	$Zr_6(\mu_3\text{-O})_4(\mu_3\text{-OH})_4$ cluster	**ftw**	1.84	57
PCN-229	$Zr_6(\mu_3\text{-O})_4(\mu_3\text{-OH})_4$ cluster	**ftw**	1.37	57
PCN-230	$Zr_6(\mu_3\text{-O})_4(\mu_3\text{-OH})_4$ cluster	**ftw**	0.53	57
MMPF-6	$Zr_6(\mu_3\text{-O})_8$ cluster	**csq**	2.28	58

[a]The new topology **ztt** of PCN-226 with Schlafli symbol $\{4\cdot8^2\}\{4^2\cdot6\cdot8^2\cdot10\}$ for the net. [b]The density was calculated on the basis of the structural models.

Electrocatalytic ORR of PCN-226. PCN-226 provides an ideal example for designing MOF electrocatalysts through chain-based structures, which could improve the chemical stability as well as increase the packing density. A close packing could further enhance the overall charge mobility via the hopping mechanism.[30−32] As a proof of concept, the electrochemical ORR catalyzed by PCN-226 was tested.

The isostructural PCN-226 series displayed excellent electroactivities toward ORR, which were assessed by cyclic voltammogram (CV) and linear sweep voltammetry (LSV) measurements (Figures S20, S21 and Table S5). As a 3D porous material, PCN-226 benefits from limited deactivation pathways as compared to molecular catalysts (Figure S22). Given the best activity, PCN-226(Co) showed a strong reversible redox wave at 0.7 V (vs reversible hydrogen electrode, RHE, Figure 3a). The LSV curve of PCN-226(Co) (Figure 3b) exhibited an onset potential of 0.83 V

https://dx.doi.org/10.1021/jacs.0c06329
J. Am. Chem. Soc. 2020, 142, 15386−15395

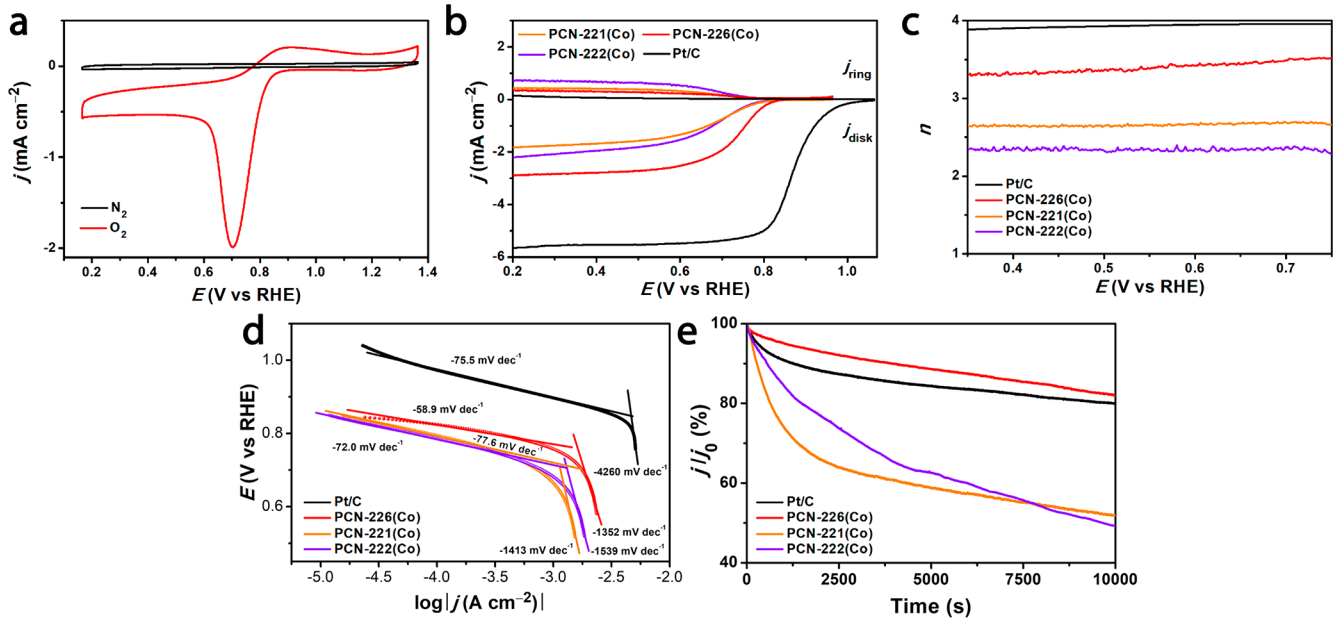

Figure 3. (a) CV curves of PCN-226(Co) in 0.1 M KOH solution saturated by N_2 and O_2, respectively. (b) LSV curves, (c) electron transfer numbers (n), and (d) Tafel plots of PCN-226(Co), PCN-221(Co), PCN-222(Co), and Pt/C. (e) Durability test at 0.46 V (vs RHE) and 1600 rpm in O_2-saturated 0.1 M KOH solution, where j_0 is the initial current. It shows PCN-226(Co) has the lowest current loss (18%), followed by Pt/C (20%), PCN-221(Co) (48%), and PCN-222(Co) (50%). The MOFs were mixed with 50% carbon black.

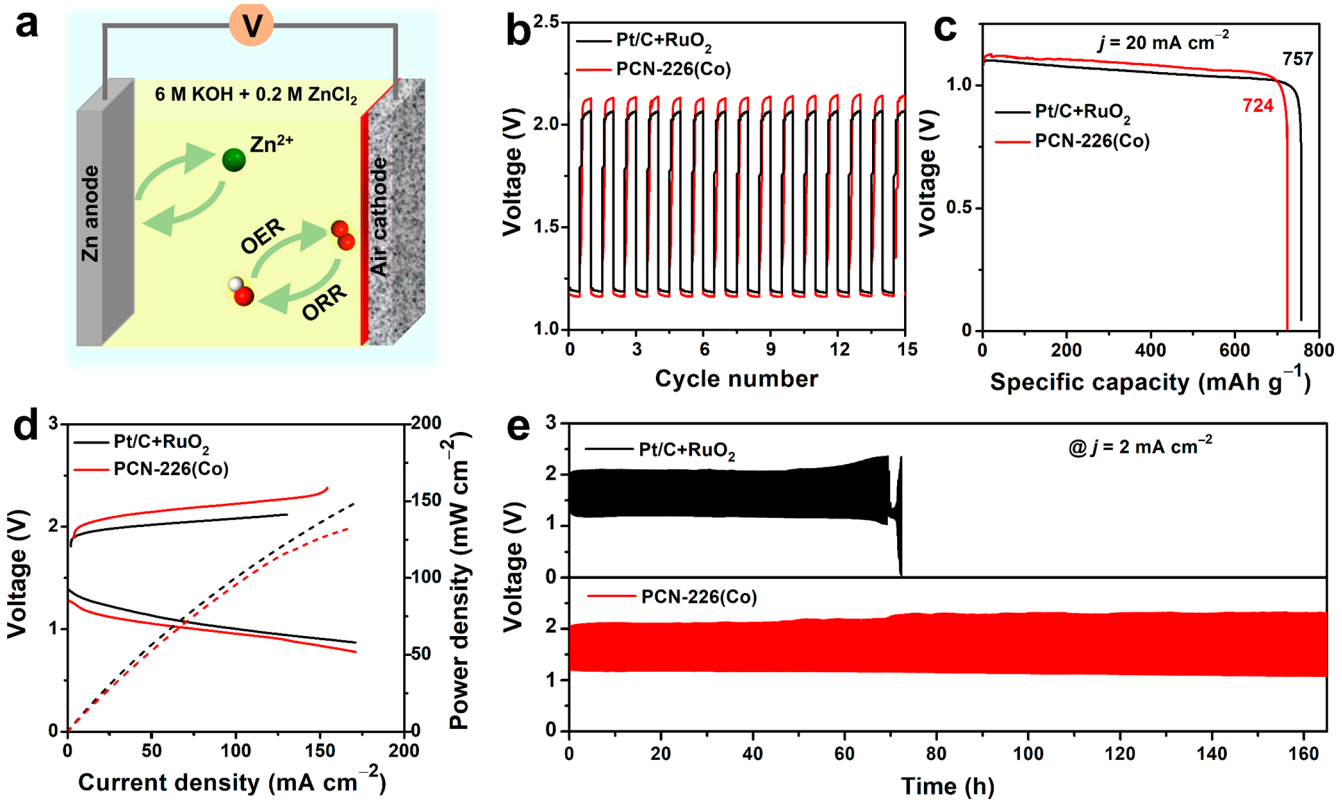

Figure 4. (a) Schematic illustration of the Zn-air battery. (b) Discharge and charge cycling curves. (c) Discharging curves at j = 20 mA cm^{-2}. (d) Polarization curves and corresponding power density. (e) Long-term durability test of the Zn-air batteries at j = 2 mA cm^{-2} assembled with PCN-226(Co) and commercial Pt/C+RuO_2. The loading of PCN-226(Co) is 6.25 times the amount that was used in the ORR test.

(E_{onset}) and half-wave potential of 0.75 V ($E_{1/2}$), while the values of pure carbon black were 0.70 and 0.62 V, respectively (Figure S23). Meanwhile, PCN-226(H_2) shows a very low activity with an $E_{1/2}$ of 0.6 V (vs RHE) (Figure S24). This result highlights the importance of the metal cations in the porphyrin as they serve as the catalytic active-sites. Notably, the potential can be further enhanced by increasing the catalyst loading (Figure S25). Because of the Zr-chain structure, the density of active metal sites in PCN-226 is so far the highest among reported porphyrinic Zr-MOFs, and it is 144% and

https://dx.doi.org/10.1021/jacs.0c06329
J. Am. Chem. Soc. 2020, 142, 15386−15395

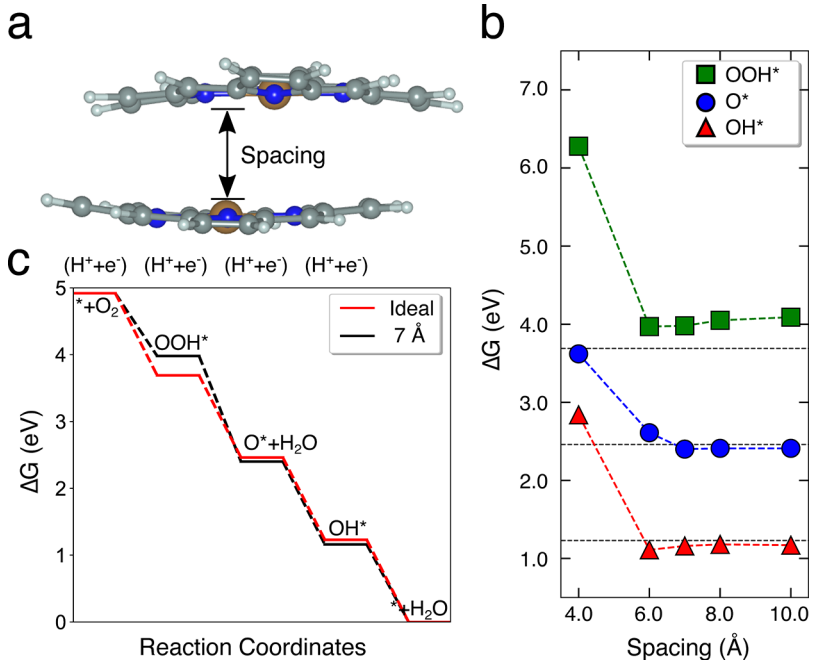

Figure 5. (a) A truncated molecular model of PCN-226. Color code: brown, Co; blue, N; gray, C; white, H. We varied the distance between the two porphyrin motifs to investigate the effect of the spacing on ORR. (b) Adsorption free energy of ORR intermediates as a function of the spacing. The two inherent spacings in PCN-226 are ca. 4 and 7 Å. The horizontal dashed lines indicate ΔG of an ideal catalyst. (c) Free energy diagram for the 7 Å spacing between porphyrin motifs (red) as compared to the ideal catalyst (black).

358% denser than the well-known PCN-221/MOF-525 and PCN-222/MOF-545, respectively (Table 1). The close packing increases the active-sites density as well as provides a better pathway for electron hopping. As a consequence, PCN-226 showed a better overall ORR activity than did cluster-based MOFs PCN-221 ($E_{1/2}$ = 0.70 V vs RHE) and PCN-222 ($E_{1/2}$ = 0.69 V vs RHE) (Figure 3b and Table S6). In addition, PCN-226 outperformed other commonly reported MOFs as ORR electrocatalysts, such as the MIL-88(Fe), ZIF-67(Co), MOF-5(Ni), and ZIF-8(Zn) (Figure S26).

Electrocatalytic ORR can be carried out in an alkaline solution through four electron ($4e^-$) and two electron ($2e^-$) pathways. Notably, the $4e^-$ selectivity provides higher reaction kinetics and can prolong the durability of the cell. The electron transfer number (n) of PCN-226(Co) was calculated as ~3.3, which indicated a mixed $4e^-$ and $2e^-$ pathways. As compared to the n number of Zr-cluster-based PCN-221 (2.6) and PCN-222 (2.3), as well as pure carbon black (2.1), PCN-226(Co) offers a better reaction pathway toward the reduction of O_2 to OH^- (Figures 3c and S27; see the Supporting Information for more details). Although the n number of PCN-226(Co) was slightly lower than that (3.9) observed for Pt/C, PCN-226(Co) provided a faster reaction kinetics as shown by the Tafel slopes (Figure 3d). As expected from the close spacing of active-sites, the reaction kinetics of PCN-226 was the fastest among the porphyrinic Zr-MOFs we tested (Figure 3d; see the Supporting Information). The calculated turnover frequency (TOF) of PCN-226(Co) at 0.2 V (vs RHE) is 0.17 e site^{-1} s^{-1}, if we assume all of the Co atoms on the electrode are available. This TOF is comparable to that of Pt/C (0.18 e site^{-1} s^{-1}) and other reported materials (Table S7). Furthermore, when we limited the deactivation pathways, PCN-226(Co) endowed a tolerance superior to methanol crossover (Figure S28). PCN-226(Co) exhibited a high durability with the lowest current loss of 18%, especially as compared to the other cluster-based MOFs (Figures 3e and S29). After the durability test, structural and compositional measurements confirmed that PCN-226(Co) remained intact, without decomposition or generation of metal oxides (Figures S30–S32).

We further evaluated the OER activity (Figure S33; see the Supporting Information for more details) and used PCN-226(Co) as air electrodes for practical applications in a rechargeable Zn-air battery (Figures 4a and S34 and movie S1). After catalysts were coated on carbon cloth to further enhance electron transfer,[59] the assembled battery exhibited an open-circuit voltage of 1.37 V (Figure S35), and the discharge and charge voltages were 1.17 and 2.14 V, respectively (Figure 4b). The specific capacity of PCN-226(Co) was 724 mAh g^{-1}, which is close to 757 mAh g^{-1} using Pt/C+RuO_2 catalysts (Figure 4c). We further compared the peak power density, which is one of the critical metrics for practical applications, to those of other electrodes. The peak power density of PCN-226(Co) was 133 mW cm^{-2}, which was comparable to the 150 mW cm^{-2} observed for Pt/C+RuO_2 (Figure 4d) and exceeded those for the previously reported state-of-the-art noble metal-free electrocatalysts, such as MOFs and MOF derived composites,[60−64] carbon materials,[11,65−69] and metal oxide composites[70−72] (Table S8). Significantly, no noticeable performance decrease was observed after 550 charge−discharge cycles over 160 h, which indicated a high electrocatalytic durability (Figure 4e).

Theoretical Calculation. As we demonstrated above, a highly dense structure could improve the performance through high catalyst loading as well as enhanced charge transfer. Single metal atom catalysts, which readily bind to the reaction intermediates of ORR, are an extreme example with infinitive distance between active-sites. As shown below, tuning the spacing between two single metal atom active-sites becomes extremely crucial for optimizing both the density of the active-sites and the reaction thermodynamics, which in turn affects

https://dx.doi.org/10.1021/jacs.0c06329
J. Am. Chem. Soc. 2020, 142, 15386−15395

the reaction kinetics. The central key is to engineer the spacing so that the binding energies of ORR intermediates, that is, OOH*, O*, and OH*, are neither too strong nor too weak. This design leads to the minimum overpotential as well as high intrinsic ORR catalytic activity.[73] To demonstrate this effect, we studied the confinement in the Co-porphyrin sites of PCN-226 using a truncated model with the same atomic coordination (Figure 5a). PCN-226 has two inherent confined spacings between the porphyrin units, that is, 4 and 7 Å. In addition to the natural spacings in PCN-226, we considered several other spacings to investigate the effect of confinement on the ORR activity. The calculated adsorption free energies (ΔG) of the ORR intermediates (O*, OH*, and OOH*) at different spacings are displayed in Figure 5b. The results show that at 4 Å spacing all ORR intermediates are significantly destabilized, which indicated that this spacing is less probable to contribute to the observed ORR activity. On the other hand, all ΔG values approach those of an ideal catalyst for spacings larger than 6 Å. The ideal spacing for ΔG_{OOH} is between 6 and 8 Å. Combined with the highly dense chain structure, this spacing explains the enhanced ORR activity observed in the case of our PCN-226 catalyst with well-defined 7 Å spacing. We further examined the effect of curvature on the ORR activity by examining a flattened model of the Co-porphyrins with 7 Å spacing, where we found negligible differences in the ΔG values of roughly 0.05 eV. The calculation results signify the importance of the spacing of active-sites on the performance in ORR.

CONCLUSIONS

We developed a new Zr oxide-chain-based MOF, PCN-226. Metalloporphyrin was incorporated in the framework, which can act as redox-active catalyst. PCN-226 demonstrates an excellent chemical stability, which enforces its compatibility in aqueous solution as electrocatalysts. We present a proof-of-concept study that highlights the importance of chain-based 3D structure in MOF design for electrochemical applications. In particular, chain-based MOFs not only allow the incorporation of close-packed, high-density redox active-sites, but also provide an opportunity to tailor the spacing between those active-sites. Thanks to this strategy, PCN-226 shows excellent electroactivity as compared to that of cluster-based MOFs. We foresee that the tunability and designability in MOF structures will promote future development on chain-based 3D MOFs as electrocatalysts. Such developments will further close the gap between reticular chemistry and materials catalysis, particularly in electrocatalysis, which contribute significantly to green energy conversion and storage.

ASSOCIATED CONTENT

Supporting Information

The Supporting Information is available free of charge at https://pubs.acs.org/doi/10.1021/jacs.0c06329.

Experimental details, PXRD, gas sorption, SEM, ICP-OES, structure refinement, XPS, electrocatalytic O_2 reduction, and DFT calculations (PDF)

Crystallographic information file for PCN-226(Cu) (CIF)

Crystallographic information file for PCN-226(Co) (CIF)

Movie S1: Recording of a Zn-air battery-powered mini car using PCN-226 as air electrodes (MP4)

AUTHOR INFORMATION

Corresponding Authors

Haoquan Zheng − *Key Laboratory of Applied Surface and Colloid Chemistry, Ministry of Education, School of Chemistry and Chemical Engineering, Shaanxi Normal University, Xi'an 710119, China;* orcid.org/0000-0003-3869-4055; Email: zhenghaoquan@snnu.edu.cn

Hong-Cai Zhou − *Department of Chemistry and Department of Materials Science and Engineering, Texas A&M University, College Station, Texas 77843-3255, United States;* orcid.org/0000-0002-9029-3788; Email: zhou@chem.tamu.edu

Zhehao Huang − *Department of Materials and Environmental Chemistry, Stockholm University, Stockholm SE-106 91, Sweden;* orcid.org/0000-0002-4575-7870; Email: zhehao.huang@mmk.su.se

Authors

Magdalena Ola Cichocka − *Department of Materials and Environmental Chemistry, Stockholm University, Stockholm SE-106 91, Sweden*

Zuozhong Liang − *Key Laboratory of Applied Surface and Colloid Chemistry, Ministry of Education, School of Chemistry and Chemical Engineering, Shaanxi Normal University, Xi'an 710119, China*

Dawei Feng − *Department of Chemistry, Texas A&M University, College Station, Texas 77843-3255, United States*

Seoin Back − *Department of Chemical and Biomolecular Engineering, Sogang University, Seoul 04107, Republic of Korea*

Samira Siahrostami − *Department of Chemistry, University of Calgary, Calgary, Alberta T2N1N4, Canada;* orcid.org/0000-0002-1192-4634

Xia Wang − *Department of Materials and Environmental Chemistry, Stockholm University, Stockholm SE-106 91, Sweden*

Laura Samperisi − *Department of Materials and Environmental Chemistry, Stockholm University, Stockholm SE-106 91, Sweden*

Yujia Sun − *Department of Chemistry, Texas A&M University, College Station, Texas 77843-3255, United States*

Hongyi Xu − *Department of Materials and Environmental Chemistry, Stockholm University, Stockholm SE-106 91, Sweden;* orcid.org/0000-0002-8271-3906

Niklas Hedin − *Department of Materials and Environmental Chemistry, Stockholm University, Stockholm SE-106 91, Sweden;* orcid.org/0000-0002-7284-2974

Xiaodong Zou − *Department of Materials and Environmental Chemistry, Stockholm University, Stockholm SE-106 91, Sweden;* orcid.org/0000-0001-6748-6656

Complete contact information is available at: https://pubs.acs.org/10.1021/jacs.0c06329

Author Contributions

[▽]M.O.C. and Z.L. contributed equally to this work.

Notes

The authors declare no competing financial interest.

The crystallographic data for PCN-226(Cu) and PCN-226(Co) have been deposited at the Cambridge Crystallographic Data Centre (CCDC, free of charge at https://www.ccdc.cam.ac.uk) under deposition numbers CCDC 2004306 and 2020844, respectively.

https://dx.doi.org/10.1021/jacs.0c06329
J. Am. Chem. Soc. 2020, 142, 15386−15395

■ ACKNOWLEDGMENTS

This research was supported by the Swedish Research Council (VR, 2016-04625, 2017-04321), the CATSS project from the Knut and Alice Wallenberg Foundation (KAW, 2016.0072), and the National Natural Science Foundation of China (grant nos. 21975148, 21808138, and 21601118). S.S. acknowledges the support from the University of Calgary's Canada First Research Excellence Fund Program, the Global Research Initiative in Sustainable Low Carbon Unconventional Resources.

■ REFERENCES

(1) Shao, M.; Chang, Q.; Dodelet, J.-P.; Chenitz, R. Recent Advances in Electrocatalysts for Oxygen Reduction Reaction. *Chem. Rev.* **2016**, *116* (6), 3594−3657.
(2) Cheng, F.; Chen, J. Metal−Air Batteries: From Oxygen Reduction Electrochemistry to Cathode Catalysts. *Chem. Soc. Rev.* **2012**, *41* (6), 2172−2192.
(3) Wang, Y.-J.; Zhao, N.; Fang, B.; Li, H.; Bi, X. T.; Wang, H. Carbon-Supported Pt-Based Alloy Electrocatalysts for the Oxygen Reduction Reaction in Polymer Electrolyte Membrane Fuel Cells: Particle Size, Shape, and Composition Manipulation and Their Impact to Activity. *Chem. Rev.* **2015**, *115* (9), 3433−3467.
(4) Chen, Z.; Higgins, D.; Yu, A.; Zhang, L.; Zhang, J. A Review on Non-Precious Metal Electrocatalysts for PEM Fuel Cells. *Energy Environ. Sci.* **2011**, *4* (9), 3167−3192.
(5) Nie, Y.; Li, L.; Wei, Z. Recent Advancements in Pt and Pt-Free Catalysts for Oxygen Reduction Reaction. *Chem. Soc. Rev.* **2015**, *44* (8), 2168−2201.
(6) Hou, J.; Wu, Y.; Zhang, B.; Cao, S.; Li, Z.; Sun, L. Rational Design of Nanoarray Architectures for Electrocatalytic Water Splitting. *Adv. Funct. Mater.* **2019**, *29* (20), 1808367.
(7) Liang, Z.; Fan, X.; Lei, H.; Qi, J.; Li, Y.; Gao, J.; Huo, M.; Yuan, H.; Zhang, W.; Lin, H.; Zheng, H.; Cao, R. Cobalt−Nitrogen-Doped Helical Carbonaceous Nanotubes as a Class of Efficient Electrocatalysts for the Oxygen Reduction Reaction. *Angew. Chem., Int. Ed.* **2018**, *57* (40), 13187−13191.
(8) Zhang, C.; Yang, H.; Zhong, D.; Xu, Y.; Wang, Y.; Yuan, Q.; Liang, Z.; Wang, B.; Zhang, W.; Zheng, H.; Cheng, T.; Cao, R. A Yolk−Shell Structured Metal−Organic Framework with Encapsulated Iron-Porphyrin and Its Derived Bimetallic Nitrogen-Doped Porous Carbon for an Efficient Oxygen Reduction Reaction. *J. Mater. Chem. A* **2020**, *8* (19), 9536−9544.
(9) Yaghi, O. M.; O'Keeffe, M.; Ockwig, N. W.; Chae, H. K.; Eddaoudi, M.; Kim, J. Reticular Synthesis and the Design of New Materials. *Nature* **2003**, *423* (6941), 705−714.
(10) Kitagawa, S.; Kitaura, R.; Noro, S. Functional Porous Coordination Polymers. *Angew. Chem., Int. Ed.* **2004**, *43* (18), 2334−2375.
(11) Yang, S.; Yu, Y.; Dou, M.; Zhang, Z.; Dai, L.; Wang, F. Two-Dimensional Conjugated Aromatic Networks as High-Site-Density and Single-Atom Electrocatalysts for the Oxygen Reduction Reaction. *Angew. Chem., Int. Ed.* **2019**, *58* (41), 14724−14730.
(12) Zion, N.; Cullen, D. A.; Zelenay, P.; Elbaz, L. Heat-Treated Aerogel as a Catalyst for the Oxygen Reduction Reaction. *Angew. Chem., Int. Ed.* **2020**, *59* (6), 2483−2489.
(13) Eddaoudi, M.; Kim, J.; Rosi, N.; Vodak, D.; Wachter, J.; O'Keeffe, M.; Yaghi, O. M. Systematic Design of Pore Size and Functionality in Isoreticular MOFs and Their Application in Methane Storage. *Science* **2002**, *295* (5554), 469−472.
(14) Aijaz, A.; Fujiwara, N.; Xu, Q. From Metal−Organic Framework to Nitrogen-Decorated Nanoporous Carbons: High CO_2 Uptake and Efficient Catalytic Oxygen Reduction. *J. Am. Chem. Soc.* **2014**, *136* (19), 6790−6793.
(15) Xia, B. Y.; Yan, Y.; Li, N.; Wu, H. B.; Lou, X. W.; Wang, X. A Metal−Organic Framework-Derived Bifunctional Oxygen Electrocatalyst. *Nat. Energy* **2016**, *1* (1), 15006.
(16) Yang, F.; Xu, G.; Dou, Y.; Wang, B.; Zhang, H.; Wu, H.; Zhou, W.; Li, J.-R.; Chen, B. A Flexible Metal−Organic Framework with a High Density of Sulfonic Acid Sites for Proton Conduction. *Nat. Energy* **2017**, *2* (11), 877.
(17) Yu, X.; Wang, L.; Cohen, S. M. Photocatalytic Metal−Organic Frameworks for Organic Transformations. *CrystEngComm* **2017**, *19* (29), 4126−4136.
(18) Yuan, S.; Qin, J.-S.; Xu, H.-Q.; Su, J.; Rossi, D.; Chen, Y.; Zhang, L.; Lollar, C.; Wang, Q.; Jiang, H.-L.; Son, D. H.; Xu, H.; Huang, Z.; Zou, X.; Zhou, H.-C. $[Ti_8Zr_2O_{12}(COO)_{16}]$ Cluster: An Ideal Inorganic Building Unit for Photoactive Metal−Organic Frameworks. *ACS Cent. Sci.* **2018**, *4* (1), 105−111.
(19) Jiao, L.; Wan, G.; Zhang, R.; Zhou, H.; Yu, S.-H.; Jiang, H.-L. From Metal−Organic Frameworks to Single-Atom Fe Implanted N-Doped Porous Carbons: Efficient Oxygen Reduction in Both Alkaline and Acidic Media. *Angew. Chem., Int. Ed.* **2018**, *57* (28), 8525−8529.
(20) Hou, C.-C.; Zou, L.; Sun, L.; Zhang, K.; Liu, Z.; Li, Y.; Li, C.; Zou, R.; Yu, J.; Xu, Q. Single-Atom Iron Catalysts on Overhang-Eave Carbon Cages for High-Performance Oxygen Reduction Reaction. *Angew. Chem., Int. Ed.* **2020**, *59* (19), 7384−7389.
(21) Sheberla, D.; Bachman, J. C.; Elias, J. S.; Sun, C.-J.; Shao-Horn, Y.; Dinca, M. Conductive MOF Electrodes for Stable Supercapacitors with High Areal Capacitance. *Nat. Mater.* **2017**, *16*, 220−224.
(22) Feng, D.; Lei, T.; Lukatskaya, M. R.; Park, J.; Huang, Z.; Lee, M.; Shaw, L.; Chen, S.; Yakovenko, A. A.; Kulkarni, A.; Xiao, J.; Fredrickson, K.; Tok, J. B.; Zou, X.; Cui, Y.; Bao, Z. Robust and Conductive Two-Dimensional Metal−organic Frameworks with Exceptionally High Volumetric and Areal Capacitance. *Nat. Energy* **2018**, *3* (1), 30−36.
(23) Park, J.; Hinckley, A. C.; Huang, Z.; Feng, D.; Yakovenko, A. A.; Lee, M.; Chen, S.; Zou, X.; Bao, Z. Synthetic Routes for a 2D Semiconductive Copper Hexahydroxybenzene Metal−Organic Framework. *J. Am. Chem. Soc.* **2018**, *140* (44), 14533−14537.
(24) Park, J.; Lee, M.; Feng, D.; Huang, Z.; Hinckley, A. C.; Yakovenko, A.; Zou, X.; Cui, Y.; Bao, Z. Stabilization of Hexaaminobenzene in a 2D Conductive Metal−Organic Framework for High Power Sodium Storage. *J. Am. Chem. Soc.* **2018**, *140* (32), 10315−10323.
(25) Day, R. W.; Bediako, D. K.; Rezaee, M.; Parent, L. R.; Skorupskii, G.; Arguilla, M. Q.; Hendon, C. H.; Stassen, I.; Gianneschi, N. C.; Kim, P.; Dinca, M. Single Crystals of Electrically Conductive Two-Dimensional Metal−Organic Frameworks: Structural and Electrical Transport Properties. *ACS Cent. Sci.* **2019**, *5* (12), 1959−1964.
(26) Yao, M.-S.; Zheng, J.-J.; Wu, A.-Q.; Xu, G.; Nagarkar, S. S.; Zhang, G.; Tsujimoto, M.; Sakaki, S.; Horike, S.; Otake, K.; Kitagawa, S. A Dual-Ligand Porous Coordination Polymer Chemiresistor with Modulated Conductivity and Porosity. *Angew. Chem., Int. Ed.* **2020**, *59* (1), 172−176.
(27) Wang, T. C.; Hod, I.; Audu, C. O.; Vermeulen, N. A.; Nguyen, S. T.; Farha, O. K.; Hupp, J. T. Rendering High Surface Area, Mesoporous Metal−Organic Frameworks Electronically Conductive. *ACS Appl. Mater. Interfaces* **2017**, *9* (14), 12584−12591.
(28) Stassen, I.; Burtch, N.; Talin, A.; Falcaro, P.; Allendorf, M.; Ameloot, R. An Updated Roadmap for the Integration of Metal−Organic Frameworks with Electronic Devices and Chemical Sensors. *Chem. Soc. Rev.* **2017**, *46* (11), 3185−3241.
(29) Roy, S.; Huang, Z.; Bhunia, A.; Castner, A.; Gupta, A. K.; Zou, X.; Ott, S. Electrocatalytic Hydrogen Evolution from a Cobaloxime-Based Metal−Organic Framework Thin Film. *J. Am. Chem. Soc.* **2019**, *141* (40), 15942−15950.
(30) AlKaabi, K.; Wade, C. R.; Dinca, M. Transparent-to-Dark Electrochromic Behavior in Naphthalene-Diimide-Based Mesoporous MOF-74 Analogs. *Chem.* **2016**, *1* (2), 264−272.
(31) Ahrenholtz, S. R.; Epley, C. C.; Morris, A. J. Solvothermal Preparation of an Electrocatalytic Metalloporphyrin MOF Thin Film and Its Redox Hopping Charge-Transfer Mechanism. *J. Am. Chem. Soc.* **2014**, *136* (6), 2464−2472.

https://dx.doi.org/10.1021/jacs.0c06329
J. Am. Chem. Soc. 2020, 142, 15386−15395

(32) Liberman, I.; Shimoni, R.; Ifraemov, R.; Rozenberg, I.; Singh, C.; Hod, I. Active-Site Modulation in an Fe-Porphyrin-Based Metal−Organic Framework through Ligand Axial Coordination: Accelerating Electrocatalysis and Charge-Transport Kinetics. *J. Am. Chem. Soc.* **2020**, *142* (4), 1933−1940.
(33) Fateeva, A.; Chater, P. A.; Ireland, C. P.; Tahir, A. A.; Khimyak, Y. Z.; Wiper, P. V.; Darwent, J. R.; Rosseinsky, M. J. A Water-Stable Porphyrin-Based Metal−Organic Framework Active for Visible-Light Photocatalysis. *Angew. Chem., Int. Ed.* **2012**, *51* (30), 7440−7444.
(34) Micheroni, D.; Lan, G.; Lin, W. Efficient Electrocatalytic Proton Reduction with Carbon Nanotube-Supported Metal−Organic Frameworks. *J. Am. Chem. Soc.* **2018**, *140* (46), 15591−15595.
(35) Kornienko, N.; Zhao, Y.; Kley, C. S.; Zhu, C.; Kim, D.; Lin, S.; Chang, C. J.; Yaghi, O. M.; Yang, P. Metal−Organic Frameworks for Electrocatalytic Reduction of Carbon Dioxide. *J. Am. Chem. Soc.* **2015**, *137* (44), 14129−14135.
(36) Dong, B.-X.; Qian, S.-L.; Bu, F.-Y.; Wu, Y.-C.; Feng, L.-G.; Teng, Y.-L.; Liu, W.-L.; Li, Z.-W. Electrochemical Reduction of CO_2 to CO by a Heterogeneous Catalyst of Fe−Porphyrin-Based Metal−Organic Framework. *ACS Appl. Energy Mater.* **2018**, *1* (9), 4662−4669.
(37) Hod, I.; Sampson, M. D.; Deria, P.; Kubiak, C. P.; Farha, O. K.; Hupp, J. T. Fe-Porphyrin-Based Metal−Organic Framework Films as High-Surface Concentration, Heterogeneous Catalysts for Electrochemical Reduction of CO_2. *ACS Catal.* **2015**, *5* (11), 6302−6309.
(38) Lu, X.-F.; Liao, P.-Q.; Wang, J.-W.; Wu, J.-X.; Chen, X.-W.; He, C.-T.; Zhang, J.-P.; Li, G.-R.; Chen, X.-M. An Alkaline-Stable, Metal Hydroxide Mimicking Metal−Organic Framework for Efficient Electrocatalytic Oxygen Evolution. *J. Am. Chem. Soc.* **2016**, *138* (27), 8336−8339.
(39) Xue, Z.; Liu, K.; Liu, Q.; Li, Y.; Li, M.; Su, C.-Y.; Ogiwara, N.; Kobayashi, H.; Kitagawa, H.; Liu, M.; Li, G. Missing-Linker Metal-Organic Frameworks for Oxygen Evolution Reaction. *Nat. Commun.* **2019**, *10* (1), 5048.
(40) Li, W.; Xue, S.; Watzele, S.; Hou, S.; Fichtner, J.; Semrau, A. L.; Zhou, L.; Welle, A.; Bandarenka, A. S.; Fischer, R. A. Advanced Bifunctional Oxygen Reduction and Evolution Electrocatalyst Derived from Surface-Mounted Metal−Organic Frameworks. *Angew. Chem., Int. Ed.* **2020**, *59* (14), 5837−5843.
(41) Usov, P. M.; Huffman, B.; Epley, C. C.; Kessinger, M. C.; Zhu, J.; Maza, W. A.; Morris, A. J. Study of Electrocatalytic Properties of Metal−Organic Framework PCN-223 for the Oxygen Reduction Reaction. *ACS Appl. Mater. Interfaces* **2017**, *9* (39), 33539−33543.
(42) Cheng, W.; Zhao, X.; Su, H.; Tang, F.; Che, W.; Zhang, H.; Liu, Q. Lattice-Strained Metal−Organic-Framework Arrays for Bifunctional Oxygen Electrocatalysis. *Nat. Energy* **2019**, *4* (2), 115−122.
(43) Zhong, H.; Ly, K. H.; Wang, M.; Krupskaya, Y.; Han, X.; Zhang, J.; Zhang, J.; Kataev, V.; Büchner, B.; Weidinger, I. M.; Kaskel, S.; Liu, P.; Chen, M.; Dong, R.; Feng, X. A Phthalocyanine-Based Layered Two-Dimensional Conjugated Metal−Organic Framework as a Highly Efficient Electrocatalyst for the Oxygen Reduction Reaction. *Angew. Chem., Int. Ed.* **2019**, *58* (31), 10677−10682.
(44) Lu, X. F.; Xia, B. Y.; Zang, S.-Q.; Lou, X. W. Metal−Organic Frameworks Based Electrocatalysts for the Oxygen Reduction Reaction. *Angew. Chem., Int. Ed.* **2020**, *59* (12), 4634−4650.
(45) Cavka, J. H.; Jakobsen, S.; Olsbye, U.; Guillou, N.; Lamberti, C.; Bordiga, S.; Lillerud, K. P. A New Zirconium Inorganic Building Brick Forming Metal Organic Frameworks with Exceptional Stability. *J. Am. Chem. Soc.* **2008**, *130* (42), 13850−13851.
(46) Cichocka, M. O.; Ångström, J.; Wang, B.; Zou, X.; Smeets, S. High-Throughput Continuous Rotation Electron Diffraction Data Acquisition via Software Automation. *J. Appl. Crystallogr.* **2018**, *51* (6), 1652−1661.
(47) Huang, Z.; Ge, M.; Carraro, F.; Doonan, C. J.; Falcaro, P.; Zou, X. Can 3D Electron Diffraction Provide Accurate Atomic Structures of Metal-Organic Frameworks? *Faraday Discuss.* **2020**, 1 DOI: 10.1039/D0FD00015A.
(48) Warren, M. 'Why Didn't We Think to Do This Earlier?' Chemists Thrilled by Speedy Atomic Structures. *Nature* **2018**, *563*, 16.
(49) Guillerm, V.; Ragon, F.; Dan-Hardi, M.; Devic, T.; Vishnuvarthan, M.; Campo, B.; Vimont, A.; Clet, G.; Yang, Q.; Maurin, G.; Férey, G.; Vittadini, A.; Gross, S.; Serre, C. A Series of Isoreticular, Highly Stable, Porous Zirconium Oxide Based Metal−Organic Frameworks. *Angew. Chem., Int. Ed.* **2012**, *51* (37), 9267−9271.
(50) Mouchaham, G.; Cooper, L.; Guillou, N.; Martineau, C.; Elkaïm, E.; Bourrelly, S.; Llewellyn, P. L.; Allain, C.; Clavier, G.; Serre, C.; Devic, T. A Robust Infinite Zirconium Phenolate Building Unit to Enhance the Chemical Stability of Zr MOFs. *Angew. Chem., Int. Ed.* **2015**, *54* (45), 13297−13301.
(51) Feng, D.; Jiang, H.-L.; Chen, Y.-P.; Gu, Z.-Y.; Wei, Z.; Zhou, H.-C. Metal−Organic Frameworks Based on Previously Unknown Zr8/Hf8 Cubic Clusters. *Inorg. Chem.* **2013**, *52* (21), 12661−12667.
(52) Morris, W.; Volosskiy, B.; Demir, S.; Gándara, F.; McGrier, P. L.; Furukawa, H.; Cascio, D.; Stoddart, J. F.; Yaghi, O. M. Synthesis, Structure, and Metalation of Two New Highly Porous Zirconium Metal−Organic Frameworks. *Inorg. Chem.* **2012**, *51* (12), 6443−6445.
(53) Feng, D.; Gu, Z.-Y.; Li, J.-R.; Jiang, H.-L.; Wei, Z.; Zhou, H.-C. Zirconium-Metalloporphyrin PCN-222: Mesoporous Metal−Organic Frameworks with Ultrahigh Stability as Biomimetic Catalysts. *Angew. Chem., Int. Ed.* **2012**, *51* (41), 10307−10310.
(54) Feng, D.; Gu, Z.-Y.; Chen, Y.-P.; Park, J.; Wei, Z.; Sun, Y.; Bosch, M.; Yuan, S.; Zhou, H.-C. A Highly Stable Porphyrinic Zirconium Metal−Organic Framework with Shp-a Topology. *J. Am. Chem. Soc.* **2014**, *136* (51), 17714−17717.
(55) Feng, D.; Chung, W.-C.; Wei, Z.; Gu, Z.-Y.; Jiang, H.-L.; Chen, Y.-P.; Darensbourg, D. J.; Zhou, H.-C. Construction of Ultrastable Porphyrin Zr Metal−Organic Frameworks through Linker Elimination. *J. Am. Chem. Soc.* **2013**, *135* (45), 17105−17110.
(56) Jiang, H.-L.; Feng, D.; Wang, K.; Gu, Z.-Y.; Wei, Z.; Chen, Y.-P.; Zhou, H.-C. An Exceptionally Stable, Porphyrinic Zr Metal−Organic Framework Exhibiting PH-Dependent Fluorescence. *J. Am. Chem. Soc.* **2013**, *135* (37), 13934−13938.
(57) Liu, T.-F.; Feng, D.; Chen, Y.-P.; Zou, L.; Bosch, M.; Yuan, S.; Wei, Z.; Fordham, S.; Wang, K.; Zhou, H.-C. Topology-Guided Design and Syntheses of Highly Stable Mesoporous Porphyrinic Zirconium Metal−Organic Frameworks with High Surface Area. *J. Am. Chem. Soc.* **2015**, *137* (1), 413−419.
(58) Chen, Y.; Hoang, T.; Ma, S. Biomimetic Catalysis of a Porous Iron-Based Metal−Metalloporphyrin Framework. *Inorg. Chem.* **2012**, *51* (23), 12600−12602.
(59) Shi, H.; Wen, G.; Nie, Y.; Zhang, G.; Duan, H. Flexible 3D Carbon Cloth as a High-Performing Electrode for Energy Storage and Conversion. *Nanoscale* **2020**, *12* (9), 5261−5285.
(60) Chen, G.; Zhang, J.; Wang, F.; Wang, L.; Liao, Z.; Zschech, E.; Müllen, K.; Feng, X. Cobalt-Based Metal−Organic Framework Nanoarrays as Bifunctional Oxygen Electrocatalysts for Rechargeable Zn-Air Batteries. *Chem. - Eur. J.* **2018**, *24* (69), 18413−18418.
(61) Kang, X.; Fu, G.; Song, Z.; Huo, G.; Si, F.; Deng, X.; Fu, X.-Z.; Luo, J.-L. Microwave-Assisted Hydrothermal Synthesis of MOFs-Derived Bimetallic CuCo-N/C Electrocatalyst for Efficient Oxygen Reduction Reaction. *J. Alloys Compd.* **2019**, *795*, 462−470.
(62) Zhao, J.-Y.; Wang, R.; Wang, S.; Lv, Y.-R.; Xu, H.; Zang, S.-Q. Metal−Organic Framework-Derived Co_9S_8 Embedded in N, O and S-Tridoped Carbon Nanomaterials as an Efficient Oxygen Bifunctional Electrocatalyst. *J. Mater. Chem. A* **2019**, *7* (13), 7389−7395.
(63) Zhong, Y.; Pan, Z.; Wang, X.; Yang, J.; Qiu, Y.; Xu, S.; Lu, Y.; Huang, Q.; Li, W. Hierarchical Co_3O_4 Nano-Micro Arrays Featuring Superior Activity as Cathode in a Flexible and Rechargeable Zinc−Air Battery. *Adv. Sci.* **2019**, *6* (11), 1802243.
(64) Cai, Z.; Yamada, I.; Yagi, S. ZIF-Derived Co_9−XNi_xS_8 Nanoparticles Immobilized on N-Doped Carbons as Efficient Catalysts for High-Performance Zinc−Air Batteries. *ACS Appl. Mater. Interfaces* **2020**, *12* (5), 5847−5856.

(65) Zhang, J.; Zhao, Z.; Xia, Z.; Dai, L. A Metal-Free Bifunctional Electrocatalyst for Oxygen Reduction and Oxygen Evolution Reactions. *Nat. Nanotechnol.* **2015**, *10* (5), 444−452.
(66) Yang, H. B.; Miao, J.; Hung, S.-F.; Chen, J.; Tao, H. B.; Wang, X.; Zhang, L.; Chen, R.; Gao, J.; Chen, H. M.; Dai, L.; Liu, B. Identification of Catalytic Sites for Oxygen Reduction and Oxygen Evolution in N-Doped Graphene Materials: Development of Highly Efficient Metal-Free Bifunctional Electrocatalyst. *Sci. Adv.* **2016**, *2* (4), No. e1501122.
(67) Hu, Q.; Li, G.; Li, G.; Liu, X.; Zhu, B.; Chai, X.; Zhang, Q.; Liu, J.; He, C. Trifunctional Electrocatalysis on Dual-Doped Graphene Nanorings−Integrated Boxes for Efficient Water Splitting and Zn−Air Batteries. *Adv. Energy Mater.* **2019**, *9* (14), 1803867.
(68) Chen, P.; Zhou, T.; Xing, L.; Xu, K.; Tong, Y.; Xie, H.; Zhang, L.; Yan, W.; Chu, W.; Wu, C.; Xie, Y. Atomically Dispersed Iron−Nitrogen Species as Electrocatalysts for Bifunctional Oxygen Evolution and Reduction Reactions. *Angew. Chem., Int. Ed.* **2017**, *56* (2), 610−614.
(69) Han, S.; Hu, X.; Wang, J.; Fang, X.; Zhu, Y. Novel Route to Fe-Based Cathode as an Efficient Bifunctional Catalysts for Rechargeable Zn−Air Battery. *Adv. Energy Mater.* **2018**, *8* (22), 1800955.
(70) Lee, D. U.; Choi, J.-Y.; Feng, K.; Park, H. W.; Chen, Z. Advanced Extremely Durable 3D Bifunctional Air Electrodes for Rechargeable Zinc-Air Batteries. *Adv. Energy Mater.* **2014**, *4* (6), 1301389.
(71) Cheng, Y.; Dou, S.; Veder, J.-P.; Wang, S.; Saunders, M.; Jiang, S. P. Efficient and Durable Bifunctional Oxygen Catalysts Based on NiFeO@MnO_x Core−Shell Structures for Rechargeable Zn−Air Batteries. *ACS Appl. Mater. Interfaces* **2017**, *9* (9), 8121−8133.
(72) Liu, Z.-Q.; Cheng, H.; Li, N.; Ma, T. Y.; Su, Y.-Z. $ZnCo_2O_4$ Quantum Dots Anchored on Nitrogen-Doped Carbon Nanotubes as Reversible Oxygen Reduction/Evolution Electrocatalysts. *Adv. Mater.* **2016**, *28* (19), 3777−3784.
(73) Xia, W.; Mahmood, A.; Liang, Z.; Zou, R.; Guo, S. Earth-Abundant Nanomaterials for Oxygen Reduction. *Angew. Chem., Int. Ed.* **2016**, *55* (8), 2650−2676.

https://dx.doi.org/10.1021/jacs.0c06329
J. Am. Chem. Soc. 2020, 142, 15386−15395